Vehicle System Dynamics Final Article October 5, 1999

Tunnel Mover Guidance and Stability

K.F. Drenth, H.B. Pacejka, C.H. Verheul
*

SUMMARY

This paper describes the analytical work done for a new type of vehicle. The vehicle is to be used inside a tube. The simple analytical model shows a roll / lateral, and yaw degree of freedom. A relatively simple condition for motion stability has been developed. Divergent instability may occur when the c.g. lies behind the point half way between the front and rear axles. Large cornering stiffness of the tyres and small wheel suspension stiffness promotes instability

Additional degrees of freedom have been defined using an ADAMS model. In this model the effect of a steering degree of freedom was examined. The automatic guidance of the vehicle by the curved inner tube wall has been investigated and the design has been optimized. The findings of the simple linear two degree of freedom model could be verified and extensions regarding full vehicle non-linear behaviour could be given.

Using the results of both models a physical prototype of the vehicle concept is built. Full scale test runs of this prototype are planned in november 1999.

1 INTRODUCTION

The underground Logistics System (in Dutch, OLS [1]) is an underground tunnel connection for transport of flower products and time-critical air freight between the Amsterdam Airport Schiphol, the flower auction in Aalsmeer and a rail terminal to be constructed near Hoofddorp. The purpose of OLS is to achieve a drastic reduction of local road transport and to realize a direct undisturbed connection. The transport through the tunnels with a diameter of 4.5 meters is realized by vehicles on inflatable rubber tyres. With respect to a rail connection this is considered a more flexible transport system. The designated vehicle speed is set to 5.5m/s. A new concept (see Figure 1) has been proposed after a number of initial studies concerning rubber mounted vehicles on flat tunnel surface. In this concept, vehicles are placed in tunnels with a circular road surface. The tunnel surface is used for both vertical and lateral positioning by placing the wheels perpendicular to the tunnel surface.

*Delft University of Technology, P.O. Box 5034, 2600 GA Delft, The Netherlands

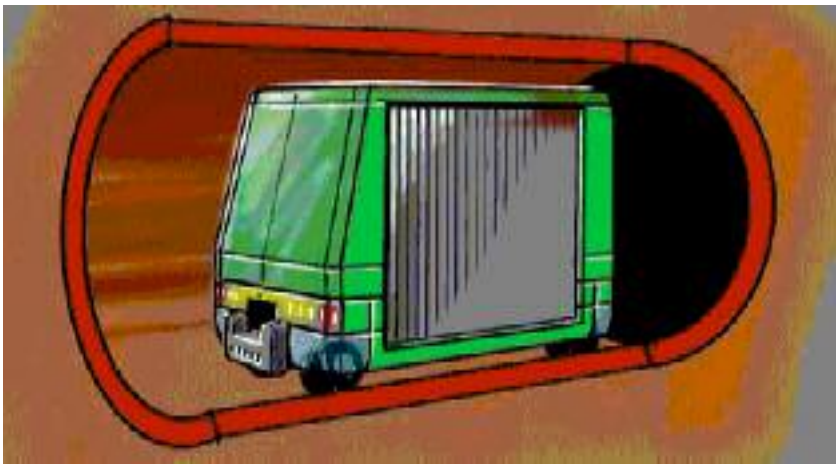

Figure 1: The vehicle concept (courtesy CTT)

The vehicle, a prototype of which is planned to be built soon, is provided with on each of the four corners a wheel set with axle and two wheels that can pivot about a longitudinal axis. The front wheel sets can be steered and are mounted slightly behind the steering axis. Steering compliance and damping elements may be added. As a result, the self-powered vehicles can run both on a flat road and inside tubes with circular cross section. Important advantages of the proposed vehicle concept are:

- Reduction of investments in tunnel infrastructure, no flat road surface or other vehicle steering mechanism is required.
- The absence of an active steering mechanism reduces accident sensitivity. The risk of blocking the tunnel by vehicles with a steering system malfunction is minimized.
- Space tolerance between vehicle and tunnel inner surface can be reduced as it is not influenced by steering errors or dynamic vehicle behaviour.
- No wheel-road contact occurs at the low part of the tunnel surface, reducing the risk of system malfunction.

Dynamic simulation models are used with increasing level of complexity to analyze vehicle stability in a wide range of concept parameters and driving speeds.

2 LINEAR MODEL

In Figure 2 the simplified system model has been depicted as used in the analytical investigation. The dimensions of the vehicle and tube have been indicated. The *tube car* runs at a constant forward speed V through a tunnel with circular cross section with radius R.

The vehicle is equipped with four sets of two wheels. Each set is mounted on an axle that can pivot about a longitudinal axis. Thereby, the wheel set will

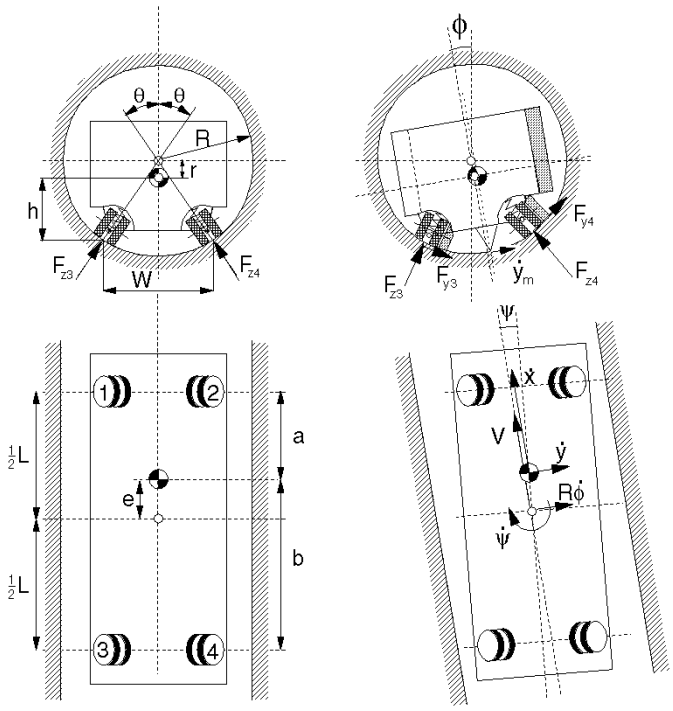

Figure 2: Tube car model dimensions and degrees of freedom

position itself perpendicularly with respect to tube inner surface. The wheelbase is denoted with L and the track width with W. The centre of gravity is located a distance e in front of the geometrical centre of the vehicle. The vehicle model is assumed to perform a motion that is limited to two degrees of freedom: the roll angle ϕ and the yaw angle ψ. The yaw angle can arise through the flexibility of the wheel suspensions normal to the tube inner surface. When yaw occurs, the front and rear wheel axles (connection lines between the centres of left and right wheel sets) show a warp angle (opposite roll) with respect to each other. Additional roll or pitch of the vehicle body through the wheel suspension flexibilities is not considered. The vehicle body is assumed to be rigid although it should be realized that the torsional flexibility of the chassis will contribute to the yaw compliance of the vehicle with respect to the tube. In the forthcoming equations of motion quantities appear which will now be defined. The side slip behaviour of the pairs of tyres per wheel set k ($k = 1, \ldots, 4$) is represented by the load dependent cornering or side slip stiffnesses C_k. Summed over the front and the rear tyres we define respectively:

$$C_f = C_1 + C_2 \ , \quad C_r = C_3 + C_4 \tag{1}$$

When moving sideways the centre of gravity, when seen from behind, describes a part of a circle with radius r. This radius expressed in terms of the tube

radius R, the height h of the centre of gravity above the wheel sets contact base plane and the track width W becomes:

$$r = \sqrt{R^2 - \frac{W^2}{4}} - h \tag{2}$$

The cosine of the angle θ of the wheel sets with respect to the upright orientation is:

$$\beta = \cos\theta = \frac{\sqrt{R^2 - \frac{W^2}{4}}}{R} \tag{3}$$

Furthermore, we have the vehicle mass m, the moments of inertia about the longitudinal and 'vertical' axes through the centre of gravity $I_{x,z}$ and the suspension radial stiffness per wheel set c_z.

The linear equation of motion for the body roll angle reads:

$$\begin{aligned}&\left(I_x + mr^2\right)\ddot{\phi} + mre\ddot{\psi} + mg(r\phi + e\psi)\\ &\quad + \tfrac{R}{V}\left[(C_f + C_r)(R\dot{\phi} - \beta V\psi) + (C_f - C_r)\tfrac{1}{2}L\beta\dot{\psi}\right] = 0\end{aligned} \tag{4}$$

and for the yaw angle:

$$\begin{aligned}&mer\ddot{\phi} + \left(I_z + me^2\right)\ddot{\psi} + mge\phi + c_z\left(\tfrac{LW}{2R}\right)^2\psi\\ &\quad + \tfrac{L\beta}{2V}\left[(C_f - C_r)(R\dot{\phi} - \beta V\psi) + (C_f + C_r)\tfrac{1}{2}L\beta\dot{\psi}\right] = 0\end{aligned} \tag{5}$$

The cornering stiffnesses are functions of the tyre normal loads as will be discussed in the subsequent section.

2.1 Tyre forces

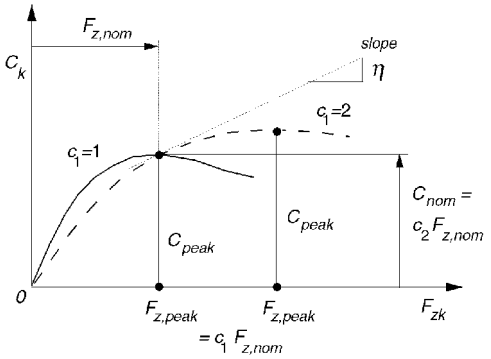

Figure 3: Cornering stiffness definition

The undisturbed normal force acting from tube surface to the set of two tyres is equal to half the vertical front or rear axle load divided by the cosine of the contact angle θ, that is: by β. A small variation will occur when the vehicle motion deviates from the steady-state rectilinear motion. The linear expressions for the side forces will not be affected by these load variations. Only the static normal forces which change through a change in vehicle weight or axle load distribution are assumed to influence the side forces at a given slip angle. This is because of the load dependency of the cornering stiffnesses. The axle vertical loads are:

$$F_{zf} = mg\frac{b}{L}, \quad F_{zr} = mg\frac{a}{L}, \quad (b = \frac{1}{2}L + e, a = \frac{1}{2}L - e) \tag{6}$$

For the wheel set normal forces we obtain:

$$F_{z1} = F_{z2} = \frac{F_{zf}}{2\beta}, \quad F_{z3} = F_{z4} = \frac{F_{zr}}{2\beta} \tag{7}$$

Assuming that the same type of tyres are mounted front and rear, the cornering stiffness for each tyre pair will be governed by the same formula. For the tyre pairs $k = 1, 2, 3, 4$ we introduce the following functional relationship with the normal load:

$$C_k = c_2 F_{z,nom} \frac{\sin\left[2 \arctan\left\{F_{zk}/(c_1 F_{z,nom})\right\}\right]}{\sin\left[2 \arctan(1/c_1)\right]} \tag{8}$$

where the nominal design load of the pair of tyres is related to the maximum vehicle weight: $F_{z,nom} = m_{max} g/4\beta$

The quantities c_1 and c_2 are the parameters; c_2 controls the level of the side slip (or cornering) stiffness and c_1 influences the derivative of C_k with respect to the tyre load F_{zk}. Figure 3 depicts the functional relationship according to (8). At $F_{zk} = F_{z,nom}$ we find for the derivative of C_k with respect to the wheel set normal load F_{zk}

$$\eta = \frac{dC_k}{dF_{zk}} = \beta \frac{dC_i}{dF_{zi}} = \frac{2c_1 c_2}{(1 + c_1^2) \tan\left\{2 \arctan\left(1/c_1\right)\right\}}, \quad k = 1, \ldots, 4; i = f, r \tag{9}$$

2.2 Analysis results

For the present study the following fixed parameter values have been used: wheel base L=4.2 m, track width W=1.7 m, c.g. height h=1.75 m, vehicle

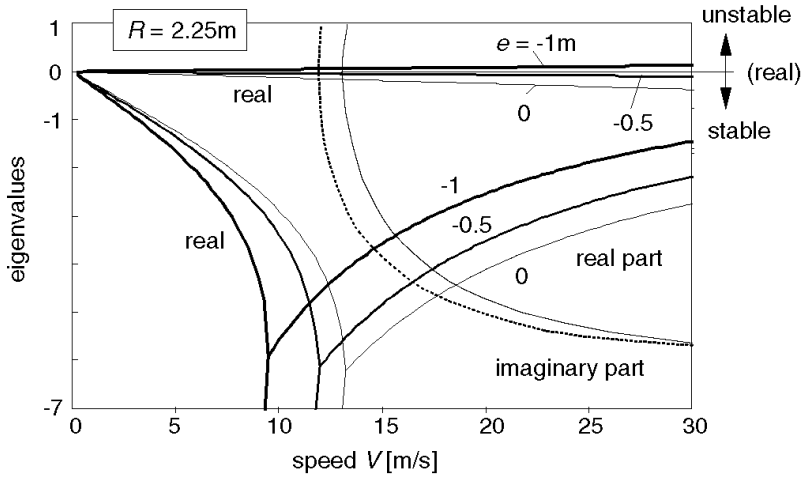

Figure 4: Roots versus vehicle speed

mass m=4000 kg, maximum vehicle mass m_{max}=5000 kg, moments of inertia I_x=4000 kgm^2 and I_z =16000 kgm^2, tyre parameters c_1=2 and c_2=15, tyre/suspension radial stiffness c_z=250000 N/m.

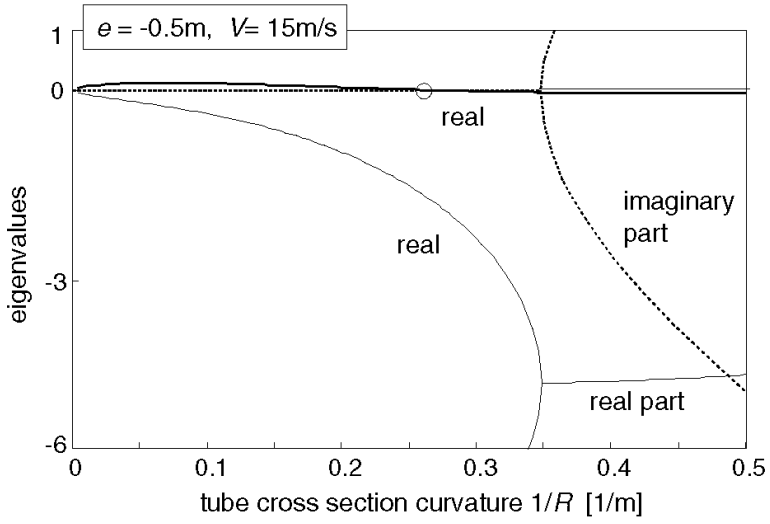

Figure 5: Roots versus tube curvature

From the eigenvalues the stability of the system is assessed. In Figure 4 the eigenvalues have been plotted for three values of the c.g. location e versus the speed of travel. The dotted lines refer to the imaginary parts and the full lines to the real parts of the possibly complex roots of the characteristic equation (that is: the eigenvalues) or to a possibly real root itself. It appears that for e = -1m and V until about 9m/s four real roots occur (one real root is negative and too large to fit in the diagram).

The imaginary components are zero. One of these real roots turns out to be positive, starting from speed equal to zero. It constitutes an unstable divergent motion (without oscillations). This instability that arises at sufficiently negative values of e appears to persist over the whole speed range with its degree of instability increasing with increasing speed. From about 9m/s onwards we have instead of the two negative real roots a set of two complex conjugate roots with a common negative real part. At larger stiffness of the suspensions and higher speeds this common part may become positive indicating that an additional oscillatory instability shows up. In Figure 5 a different presentation is shown. Here, the roots are plotted versus the tube cross section curvature. We see that at the value of e = -0.5m considered, the system is unstable until the curvature $1/R$

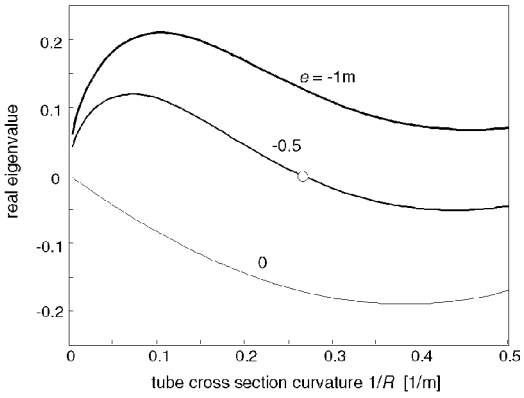

Figure 6: Real root versus tube curvature

becomes larger than about 0.27 m^{-1}. A higher boundary exists (not shown) beyond which the system is unstable again which is due to the rise of the c.g. above the tube centre line ($r < 0$) with decreasing R and fixed h and W. The variation of the real root with curvature has been shown in greater detail in Figure 6.

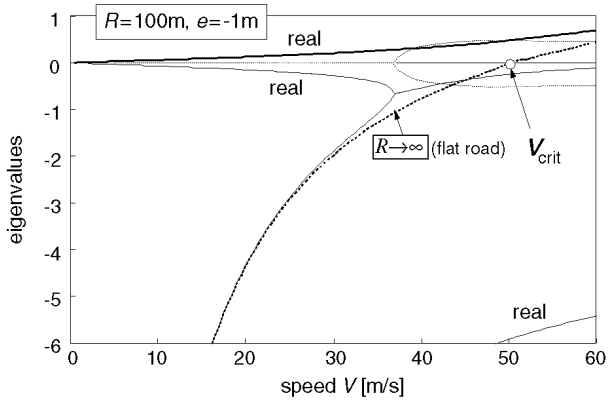

Figure 7: Roots on almost flat surface

Figure 7 represents the case of the vehicle moving over an almost flat road. On an actual flat level road surface the system shows again four roots two of which reduce to zero. The other two may either be complex or real. In the case of Figure 7 where, with the centre of gravity behind the vehicle centre and the cornering stiffness of the front tyres not much smaller than at the rear ($c_1 = 2$), the vehicle has a so-called oversteer nature. Two real roots occur, one of which may become positive. That will happen when the critical speed is surpassed. In our case the critical speed equals about 50m/s. It is known that a linear system is stable when all the Hurwitz determinants are positive. For the relatively simple fourth-order system this condition corresponds to the simpler condition that all coefficients of the characteristic equation are positive and that the third Hurwitz determinant is positive. The system will become unstable when either the last coefficient a_4 or the third Hurwitz determinant becomes negative. In our case where we find that from a stable situation the system becomes divergently unstable (that is we get a positive real root) a_4 apparently is the first to become negative. We may therefore suffice with the investigation of the possible change in sign of the last coefficient. Consequently, stability is assured if $a_4 > 0$ which yields the condition:

$$-mge^2 + \beta R\,(C_f + C_r)\,e - \frac{1}{2}\beta^2 rL\,(C_f - C_r) + \frac{1}{4}c_z r\left(\frac{LW}{R}\right)^2 > 0 \qquad (10)$$

The condition indeed appears to be independent of speed V.

For a given set of cornering stiffnesses the condition (10) can be easily evaluated. To include the effect of shifting the c.g. while accounting for the simultaneous change of the cornering stiffnesses we may employ the approximation where these quantities vary with wheel load according to the slope η (9) of the actual curve at the nominal load shown in Figure 3. If we further neglect the relatively small term with e^2 in (10) we obtain the approximate condition for

stability:

$$e > \frac{-\frac{r}{R} L^2 \sin^2\theta}{\frac{m_{max}\, g}{c_z}\left[c_2 - \eta\left\{1 - \frac{m}{m_{max}}\left(1 - \frac{1}{2}\frac{r}{R}\cos\theta\right)\right\}\right]} \tag{11}$$

Since c_2 is larger than h, we may conclude that for $r > 0$ instability may occur when $e < 0$, that is when the centre of gravity lies behind the vehicle centre. The chance for instability is greater when the tube radius R is large (then also the wheel set angle θ is small), the distance r between centre of gravity and tube centre is small, the wheel base L is small and the static deflection of the tyre/wheel suspension is large. Furthermore, it turns out that a large c_2 (i.e. large cornering stiffness), a small η (i.e. a small c_1 which means a small slope in Figure 3) and a more heavily loaded vehicle may lead to instability if $e < 0$.

3 NON-LINEAR ADAMS MODEL

3.1 Model description

A three dimensional ADAMS model was made of the vehicle containing 13 degrees of freedom. The model is defined such that comparison to the results of the 2-DOF model will be possible. For a more generic approach, the suspension vertical stiffness is related to h_{stat}, defined as the vertical deflection of the vehicle at the defined maximum vehicle mass. The relation between c_z and h_{stat} reads: $c_z = (m_{max} g)/(n h_{stat})$, with g the gravity acceleration and n the number of wheels in the vehicle. In a number of simulations, the value of h_{stat} will be varied. Both standard and dedicated model components are applied to model

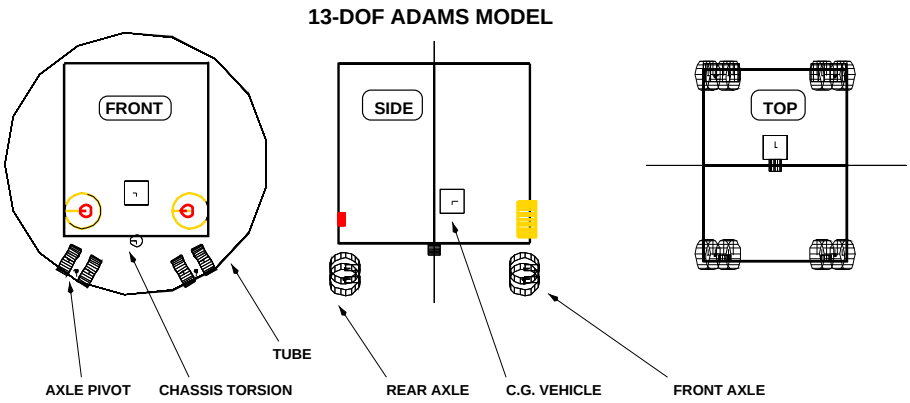

Figure 8: Overview of the ADAMS tube car model

the following components:

- **Vehicle inertia** The body of the vehicle plus pay load mass and inertia is modeled as one single 3-Dimensional body defining 6 degrees of freedom.

Table 1: Parameters for the ADAMS model

name	**value**	**units**	**explanation**
R_t	2.25	m	tube inner radius
e	0.3	m	forward shift of vehicle c.g.
L	4.2	m	vehicle wheel base
W	1.75	m	vehicle track width
h	1.5	m	height of c.g. above flat road
h_{stat}	0.03	m	tyre deflection at maximal load
m	8.3×10^3	kg	full loaded vehicle mass
m_{max}	10×10^3	kg	maximum vehicle mass
i_x	0.8	m	inertia radius ($I_{xx} = m{i_x}^2$)
i_z	1.5	m	inertia radius ($I_{zz} = m{i_z}^2$)
c_1	2.0		tyre stiffness vs. tyre load
c_2	15.0		nominal tyre slip stiffness
t	0.1	m	front wheels trail
y_{stub}	0.25	m	half wheel spacing
z_{stub}	0.11	m	offset pivot axle
R_{free}	0.25	m	free tyre radius
C_{st}	1000.0	Nm/rad	steering torsion stiffness

The centre of gravity of the vehicle body can be moved independent from the location of front and rear axles and position of the vehicle in the tube.

- **Axle suspensions** The vehicle has eight wheels, mounted two-by-two on front and rear axles pivoting around the vehicle drive direction. One degree of freedom is defined for each axle pivot angle which is controlled using a progressive spring torque table. Zero drive slip is assumed, relating the spin velocity of the wheels to the vehicle speed. Steering is defined at the front axles by an extra rotational degree of freedom about the vertical axis. In vertical direction, only tyre radial deformation is assumed in the suspension.
- **Steering system** The steering system is represented by two rotational spring/dampers. One spring is defined between the left and right axle steering angle, the other spring represents the steering system stiffness.
- **Tyre contact** The tyre lateral slip forces are calculated using the method and parameters defined in Section 2.
- **Tube geometry** The circular tube surface is modeled using an analytical description. The model uses a local reference point at the centre line of the tube for each of the wheels on the vehicle. An iteration algorithm calculates the local coordinate along the tube centre line with an accuracy of 0.1mm. The location and orientation of the contact patches *wheel-to-tube* are derived from a lookup table relating the global coordinates to local tube coordinates of the contact points.

The model is shown in Figure 8. Model parameters are listed in Table 1. The second column lists the reference settings of the model. For comparison with the 2-DOF model, the suspension settings are modified so that both wheels in an axle pivot are at identical location and the axle pivot is at the contact point.

4 RESULTS OF THE COMPLEX MODEL

Both linear analysis and time domain simulations are performed for verification of the model to the 2-DOF model, for evaluation of the effects of added model complexity and for component analysis purposes.

4.1 Comparison to 2-DOF model

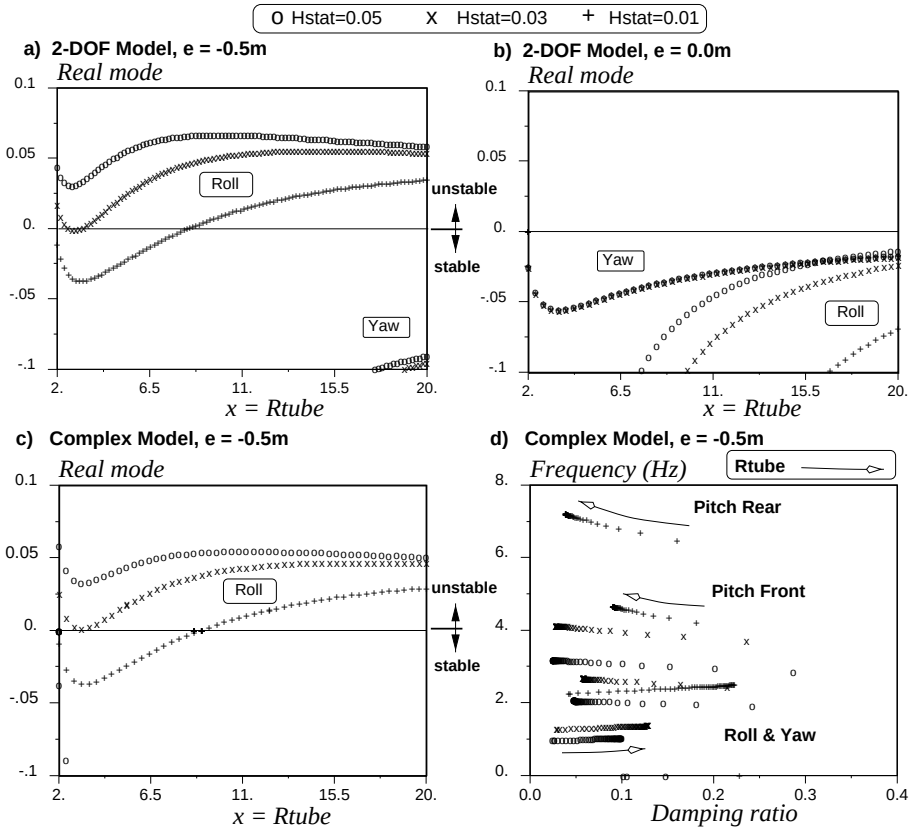

Figure 9: Linear analysis results of both the 2-DOF and the complex model

Linear analysis is used to compare the fully loaded complex model to the 2-DOF model. In Figure 9 stability curves are shown for both models. The stability curves are plotted against the radius of the tube. In view of the modeling differences between the two models, the agreement of the roll-instability is very good.

Other interesting observations based on Figure 9 are:

- The results confirm that an increase of suspension stiffness c_z (decrease of h_{stat}) will improve vehicle stability.

- The decrease in damping of the yaw mode in Figure 9.b with respect to Figure 9.a is caused by a change in front/rear axle load distribution.
- In Figure 9.a the yaw mode is just visible, in Figure 9.c and Figure 9.d this real mode is outside the applied axis limits. The differences may be explained by the fact that the 2-DOF model ignores additional roll due to deflections.
- Figure 9.d shows the Frequency-Damping loci of the low frequency oscillatory modes of the complex model. The curves denote that the damping in the two pitch modes decreases at increasing tube radius. The damping for the combined roll & yaw mode however increases with the radius of the tube.

The results show that the 2-DOF model adequately describes the dominating roll instability mode of the system. The other full vehicle modes are not described or differ from the complex model. As the 2-DOF model is 30 times faster than the complex model, it is suitable for a first analysis of vehicle stability and its dependency on global vehicle parameters.

4.2 Effect of steering system parameters

A finite steering stiffness C_{st} will reduce the effective front axle cornering stiffness, causing the vehicle to become more understeered. Main goals for a steering system parameter investigation are to analyze changes in vehicle stability and to find appropriate parameters for stable vehicle response.

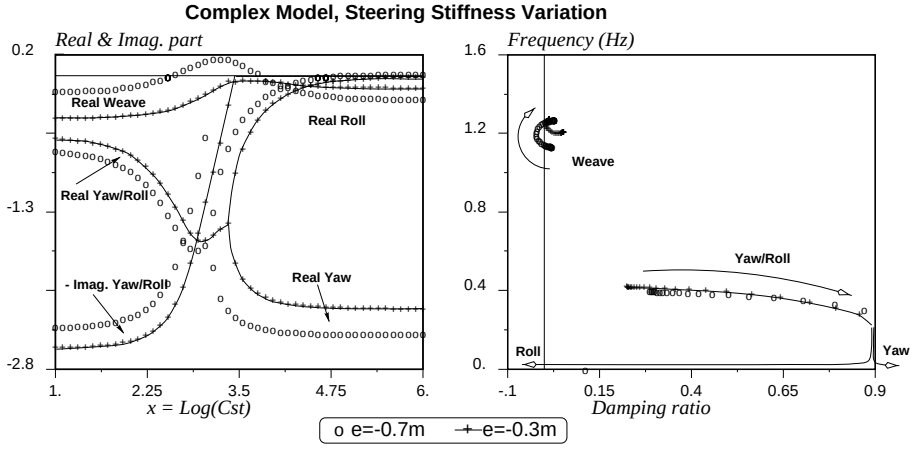

Figure 10: Variation of steering stiffness for two values of e

The results of variation of the steering stiffness at steering damping R_{st} = 100Nms/rad are presented in Figure 10. At e = -0.7 m, an oscillatory *Weave* instability occurs around C_{st} = 1000Nm/rad. Results indicate that for values of $e > -0.3$m the instability will not occur. The stability curves in the left plot approach the value for infinite steering stiffness, which represents the reference model. For decreasing values of C_{st} the monotonous unstable *Roll* mode will become stable. Around C_{st} = 1000Nm/rad an oscillatory unstable *Weave* mode

occurs of approximately 1.2 Hz. At further decrease of C_{st}, the *Roll* mode and the stable *Yaw* mode combine into a highly damped oscillatory *Yaw/Roll* mode at 0.4 Hz.

Variation of R_{st} (not included) indicates that for $R_{st} = 0$ the *Weave* instability persists until zero steering stiffness. However, at $R_{st} > 400$Nms/rad the weave instability is fully suppressed. It is interesting to notice that the range for C_{st} where the weave instability occurs appears to be optimal for curve handling in case of positive e values.

4.3 Time domain simulation results

A 90^o curve to the right side with radius $R_c = 150$m is simulated at $V = 5.5$ m/s. As the vehicle is still in prototype stage, no measurement data are available. Thus, the vehicle stability and component behaviour is assessed using dynamic simulations only. Parameter variation results are related to the results of the model reference setting (see Table 1). A number of vehicle stability indicators are used to monitor changes in overall vehicle stability and vehicle component load.

- **Steering stiffness** At infinite steering stiffness, the vehicle tends to go straight ahead and *climb* against the wall in curves. This effect is proportional to the tyre cornering stiffness. The results of the steering stiffness variation are shown in Figure 11. The following observations can be made:
  - **Roll resistance** Figure 11 indicates that at $C_{st} = 1 \times 10^4$Nm/rad curving resistance is significantly bigger than for the other runs.
  - **Steering torque** The plots in Figure 11 show a steering torque of approximately 15Nm at $C_{st} = 1 \times 10^3$Nm/rad.
  - **Lateral shift** The vehicle rolls towards the inside of the curve. The amount of roll is proportional to the lateral shift to the outside of the curve. Run $C_{st} = 1 \times 10^2$Nm/rad shows a minimal shift and a low damping of the shift. Thus, $C_{st} = 1 \times 10^3$Nm/rad is considered a reasonable value.

  The effect of variation in steering damping R_{st} was investigated. Results are not included as the simulations indicate that, for a stable model, the effect of steering damping is minimal.
- **Trail** Front wheel trail is varied from 0.01m to 0.15m. As expected, for small trail values ($t = 0.01$m) the behaviour approaches that of a high steering stiffness. The results show that a trail value between 0.05m and 0.1m is reasonable.
- **Vehicle speed** Runs are performed for $V = 4.5$, 6.5 and 8.5m/s. The results indicate no sudden changes in responses. Steady state values of steering torque and unloading of axle pivots are hardly affected. Changes in transient cornering behaviour do not indicate dangerous situations too occur.
- **Position c.g.** As already discussed, parameter e highly effects the change in oversteer / understeer. Results of variations of e are shown in Figure 12. The plots confirm that at low values of e the vehicle shows more oversteer (decrease of angle of attack and steering angle). Also, the cornering resistance

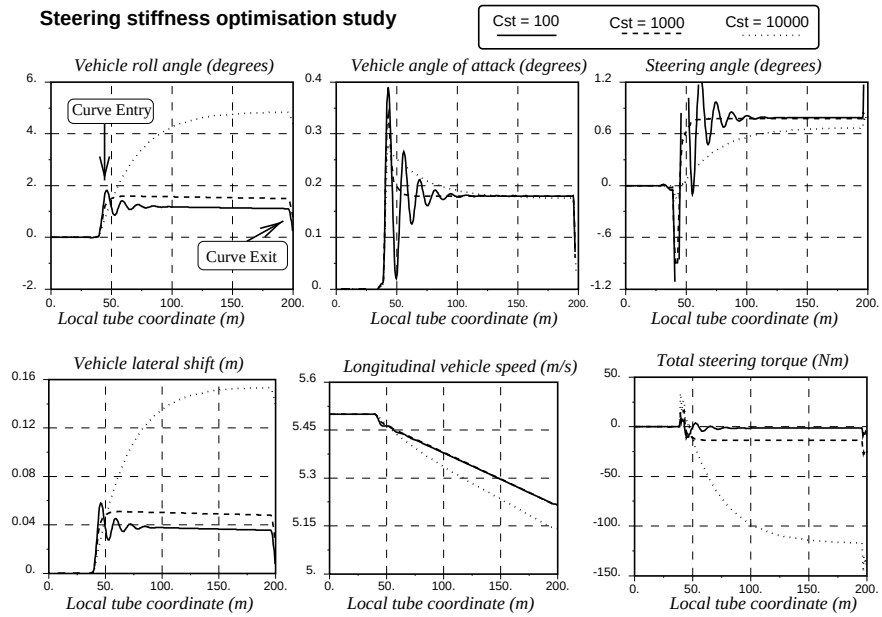

Figure 11: Steering stiffness variation results

will increase at low e values. This is an extra argument to design for a positive value of e.

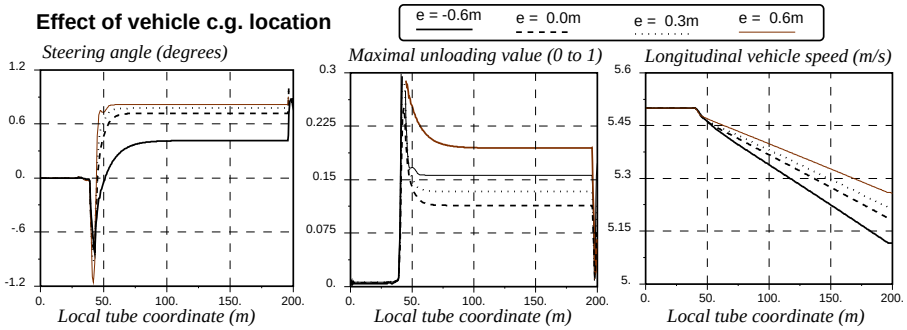

Figure 12: Effect of horizontal position centre of gravity

- **Pivot parameters** No unloading of the pivots will occur when the pivot axle is at the tyre-tube contact height. Therefore, this is the optimal place for force introduction. As this is impossible to construct, the pivot axle will be somewhere between the road surface and the wheel centre points. Other effects visible in the plots are oversteer and understeer due to changes in tyre load variation and thus cornering stiffness. The amount of instability (due to unloading) is caused by the lateral tyre slip forces. This instability is counteracted by the difference in wheel loads. Thus, a large distance between wheels on one axle pivot has a decreasing effect on the unloading instability.

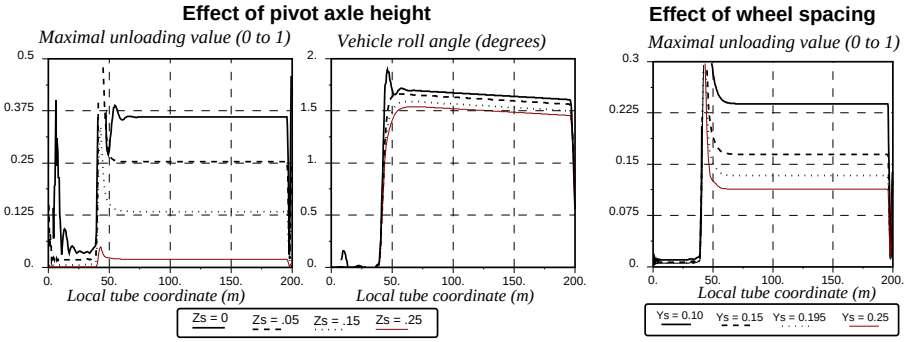

Figure 13: Effects of pivot parameters to vehicle stability

5 CONCLUSIONS

The following conclusions are drawn from this virtual prototyping project.

- The results of linear analysis with the 2-DOF model give a good agreement with the multi-body model. The monotonous vehicle instability is predicted with a high accuracy when comparing with the complex model.
- Using both models has lead to invaluable insight in the dynamic behaviour of this new vehicle concept.
- The vehicle will demonstrate an unstable roll mode, main contributing parameters are the x-location of the vehicle c.g. and the vehicle yaw stiffness.
- At a finite steering stiffness, an oscillatory weave instability may occur for negative vehicle c.g. x-location. This instability can be compensated using an adequate amount of steering damping.
- For component analysis, the use of a multi-body based simulation model has large advantages due to the possibility of re-using models and model components in a modified system layout.

REFERENCES

1. Dunselman, J.R., Pielage, B.A., Rijsenbrij, J.C., *Transporttechniek en Besturingssysteem Ondergronds Logistiek Systeem Aalsmeer-Schiphol-Hoofddorp*, (in Dutch) TRAIL Onderzoekschool - CTT publicatiereeks 39, Delft/Rotterdam, februari 1999
2. H.B. Pacejka (Ed.). Tyre Models for Vehicle Dynamics Analysis. *Proceedings of the 2nd International Colloquim on Tyre Models for Vehicle Dynamics Analysis held in Delft, The Netherlands, Oktober 21-22,1991. Supplement to Vehicle System Dynamics, Volume 21*, Amsterdam/Lisse, 1993, Swets & Zeitlinger.